Mass Flow Rate Assessment in Capillary Tubes of Refrigeration Cycle Powered by Solar Energy Using Back Propagation Artificial Neural Network

Ayman A. Aly[1, 2,*], B. Saleh[1, 2], Awad M. Aljuaid[1], Ageel F. Alogla[1], Mosleh M. Alharthi[3], and Y.S. Hamed[4,5]

[1]*Mechanical Engineering Department, College of Engineering, Taif University, PO Box 888, Taif, Saudi Arabia.*

[2]*Mechanical Engineering Department, Faculty of Engineering, Assiut University, PO Box 71516, Assiut, Egypt.*

[3]*Electrical Engineering Department, College of Engineering, Taif University, PO Box 888, Taif, Saudi Arabia.*

[4]*Physics and Engineering Mathematics Department, Faculty of Electronic Engineering, Menoufia University, Menouf PO Box 32952, Egypt.*

[5]*Mathematics and Statistics Department, Faculty of Science, Taif University, P.O. Box 888,Taif, PO Box 888, Saudi Arabia.*

Corresponding author E-mail: draymanelnaggar@yahoo.com
(*Corresponding author)

Abstract

The refrigeration systems driven by solar energy are mainly consists of photovoltaic panels, DC motor, electronics of regulation and an electrical refrigeration cycle. Capillary tubes are usually utilized in air conditioning units and domestic refrigerators for refrigerant expansion. The correlation of controlling parameters of the refrigerant mass flow rate across adiabatic straight capillary tubes is essential. Many experimental and theoretical studies have been conducted to estimate mass flow rate into adiabatic capillary tubes using non-dimensional analyses. However, the accuracy of these correlations in estimating mass flow rate is very limited. In the present paper, the mass flow rates of R22 and its alternative R407C-R600a-R290 mixture across adiabatic straight capillary tube is estimated using back propagation artificial neural network (BP-ANN). Three BP-ANN models are constructed using two methods; the first method is used to establish two individual networks for each refrigerant, and the other method is used to establish a third general network for the two inspected refrigerants together. The training of the BP-ANN is achieved using previously published measurements. The results of these three BP-ANN models exhibited high accuracy in estimating refrigerant mass flow rate in comparison with experimental measurements. The two models have shown relative differences for R407C-R600a-R290 mixture and R22 within ±0.016%, and ±0.02%, respectively. On the other hand, for the general model, the relative differences are within ±0.02%. Furthermore, the three models are examined in the predictive mode as well. The differences of the two models and the general model in the predictive mode are within ±0.5%, +0.38%/+0.41%, and -1.28%/-1.32% for R22, R407C-R600a-R290 mixture, and for the two refrigerants together, respectively. The impacts of some selected parameters, i.e. condenser temperature, degree of subcooling, and capillary tube length and diameter on the mass flow rate across the capillary tube are investigated and discussed as well.

Keywords: Artificial neural network; Capillary tubes; R22; Refrigeration cycle; R407C-R600a-R290 mixture.

1. INTRODUCTION

The refrigeration system driven by solar energy mainly consists of photovoltaic panels, DC motor, electronics of regulation and an electrical refrigeration cycle as shown in Fig. 1. Presently, the photovoltaic (PV) cells are in the market in various power ranges, efficiencies and prices and are increasingly adopted. Solar cells produce direct current electricity from sunlight. The traditional vapor compression refrigeration (VCR) cycle is the most widely spread technology available on the market for both refrigeration applications and air conditioning. It can be driven by solar energy using PV module. The main advantages of the VCR cycle driven by solar energy are its simple design and effective. The system can be used in remote areas far from the electricity grid if the required cooling capacity is modest. The VCR system uses a refrigerant circulating in a closed system through its different components. Some household, food and vaccine transportation and medical applications are the existing applications for such systems. The throttling device is a significant element in the VCR cycle. Short tube orifices, capillary tubes, electronic expansion valves, and thermostatic expansion valves are utilized for throttling refrigerant in the VCR cycles. Capillary Tubes are commonly utilized as throttling devices in freezers, air conditioners and domestic refrigerators [1-3]. The capillary tube is made of copper with a length commonly ranged from 1m to 6m, and internal diameter ranged from 0.5 mm to 2.0 mm [4]. The freezers and household refrigerators use capillary tubes to connect the inlet of evaporator and the exit of condenser with internal diameters equal to 0.787 mm or 0.711 mm [5]. It separates the high- and low-pressure sides in the refrigeration cycle. In the off-cycle periods, the capillary tube permits the cycle two pressures to equalize. This leads to decrease the required compressor starting power [6]. The capillary tube has many

advantages like simplicity, low starting compressor power, low cost, and highly reliable, with no need for maintenance. These advantages of the capillary tube make it more widespread than other expansion devices. However, the main disadvantage of the capillary tube is its non-suitability with large load variations. The flow characteristic inside the capillary tube is complicated and under normal working conditions contains phase change and non-equilibrium phenomenon. Due to those obstacles, it is difficult to guess precisely the pressure drop and mass flow across the capillary tube. Hydrocarbons (HCs), Hydrofluorocarbons (HFCs) and their mixtures are considered as alternate refrigerants instead of chlorofluorocarbons (CFCs) and hydrochlorofluorocarbons (HCFCs) in VCR cycles due to their zero-ozone depletion potential (ODP) [7].
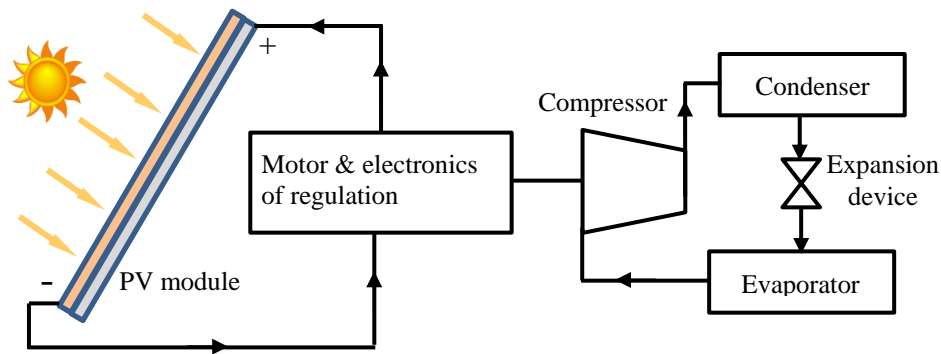
Fig. 1. Vapor compression refrigeration system driven by solar energy.

Several mathematical and experimental researches have examined the adiabatic capillary tubes performance. The impact of capillary tube diameter, length, condenser pressure, and degree of subcooling (T_{sub}) on the refrigerant mass flow rate ($\dot{m}$) is examined experimentally using R600a, R12, and R134a by Melo et al. [8]. They developed an empirical correlation to calculate the refrigerant $\dot{m}$ across the capillary tube. The refrigerant $\dot{m}$ in an adiabatic straight capillary tube using R407C, R-507A, R-404A, and R-22 is measured experimentally by Melo et al. [9]. Apaydin and Heperkan [10] and Schenk and Oellrich [11] investigated experimentally the performance of capillary tube using R600a. R134a $\dot{m}$ into adiabatic and non-adiabatic capillary tubes is studied experimentally by Dirik et al. [12]. Meyer and Dunn [13] measured experimentally the $\dot{m}$ of R134a, R22, R410A, and R407C into an adiabatic capillary tube.

Numerous semi-empirical and empirical correlations to guess the $\dot{m}$ across the adiabatic capillary tubes have been established. Wolf et al. [14] established two empirical correlations for estimation the $\dot{m}$ across the capillary tube for vapor-liquid mixture and subcooled entrance conditions utilizing the Buckingham π theorem. They used the measurements of R410A, R22, and R134a to develop the model. An empirical correlation utilizing dimensionless groups for the capillary tube using R410A, R407C, and R22 is developed by Kim et al. [15]. The dimensionless correlation depicted the measurements within relative differences ±15%. Two correlations using Buckingham π theorem to calculate the $\dot{m}$ across adiabatic capillary tube based on their measurements and data from literature is established by Choi et al. [16, 17]. Zhang [18] combined artificial neural network (ANN) method and dimensional analysis to construct a correlation to calculate the $\dot{m}$ across the adiabatic capillary tube. A general empirical correlation to guess the refrigerant $\dot{m}$ across adiabatic helically coiled and straight capillary tubes is developed by Rasti and Jeong [19, 20]. The average absolute deviation of the correlations is within ±15%. Javidmand and Hoffmann [21] performed dimensional analysis on numerical data to guess the critical $\dot{m}$ of R134a, R12, and R22 flowing across capillary tubes with various operation conditions and tube geometry. The average deviation of the estimated $\dot{m}$ utilizing the general correlations from the measurements is lower than 0.2% for the three refrigerants. Yang and Wang [22] established a general correlation to estimate refrigerant $\dot{m}$ across adiabatic capillary tube using approximate analytic solutions utilizing the data of R290, R12, R134a, R22, R600a, R404A, R410A, and R407C. The correlation results attained a Standard Deviation (SD) of 9.02% and an average deviation of -0.83% from the data. A general local power-law correlation for $\dot{m}$ across capillary tubes or short tube orifices for supercritical and subcritical entrance conditions is suggested by Yang and Zhang [23]. Approximately 2000 measurement sets of $\dot{m}$ data for R22, R12, R600a, R407C, R134a, R410A, R404A, and R744 are used from literature to develop the model. The average and SD of the model results in comparison of the data from literature are 0.8% and 8.98%, respectively. A generalized correlation for refrigerant $\dot{m}$ across adiabatic capillary tube using dimensional analysis and multi-layer perceptron neural network is suggested by Zhanga and Zhao [24]. The

deviations between the trained results of ANN and the experimental results are within ±10%. A model for guessing the refrigerant ṁ across coiled capillary tube in a split air conditioner utilizing R22 and R290 is presented by Zhou et al. [25]. Deviations of the model results from the measurements are within 8.63%. An experimental study on the flow characteristics of R22 and its alternative R407C-R600a-R290 mixture in adiabatic capillary tubes is conducted by Jabaraj et al. [26]. They studied the impact of capillary tube diameter and length, condensing pressure, and T_{sub} on the refrigerant ṁ across the capillaries. They established a non-dimensional correlation for estimating the refrigerant ṁ across the capillary tubes for various capillary tube geometries, working conditions, and refrigerant properties. The correlation guesses the ṁ of R407C-R600a-R290 mixture and R22 within average deviations of -0.11% and 0.618% and mean deviations of 4.45% and 5.54%, respectively.

From the above discussion, utilizing common estimation models based on Buckingham π theorem or applying neural network on dimensionless groups yielded big difference between the calculated and measurements of ṁ values across capillary tubes. For design and control objectives, a precise model for estimating ṁ will be very beneficial. Thus, a new method is needed to outdo the shortcomings of the common estimation models. Accordingly, in the present research, ANN method will be utilized to estimate the ṁ across adiabatic straight capillary tubes. It is reported that mixing of R407C with 20% HC could enhance the performance of the refrigeration system. It is found that the coefficient of performance (COP) of R407C-R600a-R290 mixture is greater than that obtained using R22 by nearby 11% [26]. The only drawback against the R407C-R600a-R290 mixture is its high condensing pressure, which is about 15% greater than that of R22. The purpose of this paper is to establish two individual models and one general model to estimate R22 and its alternatives R407C-R600a-R290 mixture ṁ across adiabatic straight capillary tubes utilizing ANN method. The measurements from Jabaraj et al. [26] will be utilized to establish and validate the three models.

2. THE MASS FLOW MATHEMATICAL MODEL

The first step in the mathematical model is selection of the parameters, which have obvious effects on the refrigerant ṁ across capillary tube. The selected parameters are (1) the capillary tube geometric parameters, which include capillary tube length (L) and diameter (D), (2) inlet conditions, which include inlet pressure (P_i) and T_{sub}, and (3) refrigerant properties, which include liquid viscosity (μ_f), liquid specific heat (C_{Pf}), liquid specific volume (v_f), heat of vaporization

(h_{fg}), and surface tension (σ). Since the choked flow conditions are easily come across the capillary tube at steady-state operations, the outlet pressure is not considered among the investigated parameters. These nine independent parameters are selected because of their significance in the refrigerant ṁ through the capillary tube. Consequently, the correlation for refrigerant ṁ across adiabatic straight capillary tube can be expressed using the nine parameters as follows;

$$\dot{m} = f\left(L, D, P_i, T_{sub}, v_f, \mu_f, C_{Pf}, h_{fg}, \sigma\right) \qquad (1)$$

The BP-ANN method is utilized to establish the correlation between significant nine parameters and the refrigerant ṁ. The BP-ANN models are trained to calculate the refrigerant ṁ across capillary tube at various working conditions based on the experimental measurements of R22 and R407C-R600a-R290 mixture by Jabaraj et al. [26]. Three BP-ANN models are suggested, two of them are used to inspect each refrigerant and the third is used for the two inspected refrigerants together. The refrigerants properties during the course of calculations are extracted from REFPROP 9.1 [27].

3. THE BP-ANN METHOD

Popularity of BP-ANN methodology increased these days over several constraints of verities strategies in modelling of different framework. BP-ANN procedures are utilized correctly to simulate complicated physical systems in different fields consisting of engineering physics. BP-ANN methodologies aid relating system parameters for instances wherein the traditional polices can't describe satisfactorily in an actual duration structure [28-30].

Orientation of BP-ANN strategies, which are established and trained from measurements, usually reveals modifications of net weights and biases in order to minimize the deviations of the network and the target outputs. The input factors are normalized to overcome the effect of its various dimensions and ranges.

Figure 2 presents the structure of the BP-ANN framework. The first layer accommodates 9 inputs variables related to neurons within the second layer via the assigned weights for every connection. In the hidden layer, the neurons (1:50), are determined by updating the networks (NW) to eliminate the deviation. The last layer is the output layer with one neuron y. The ANN method of modelling real systems takes into consideration as a shape of complicated regression version of unknown system.

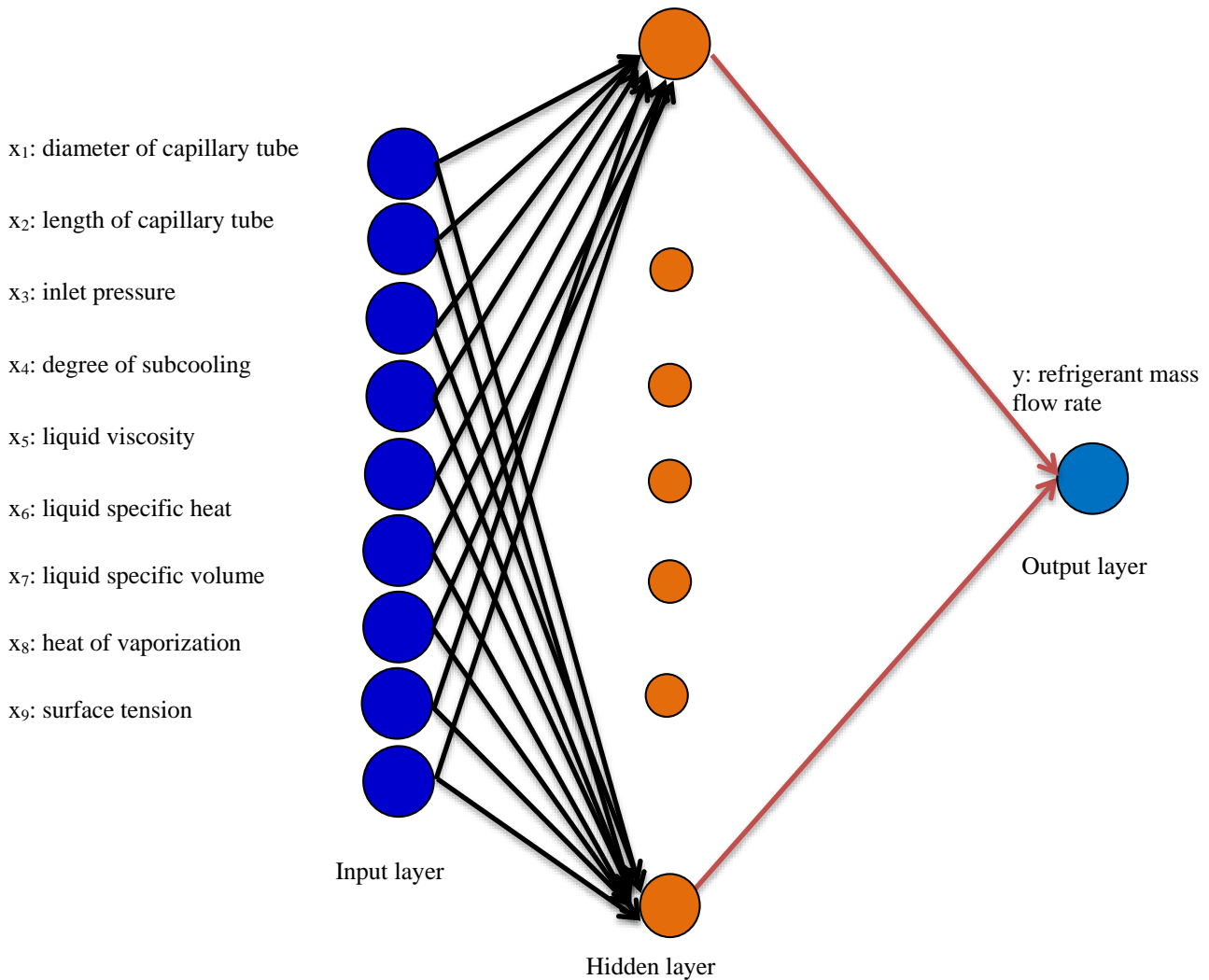**Fig. 2.** Structure of the BP-ANN.

The ANN functions can be calculated as follow:

$$y = g_A \left(\sum_{i=1}^{50} z_i \beta_j + \emptyset \right) \quad (2)$$

$$z_j = f_A \left(\sum_{i=1}^{9} x_i w_{ij} + \tau_j \right) \quad (3)$$

Where

τ_j is the neuron z_j bias

$\emptyset$ is the output y bias.

w_{ij} is the connection weight from neuron x_i to neuron z_j

β_j is the connection weight from neuron z_j to y.

and g_A and f_A are energizing mappings that generate continuous values instead of discrete values.

The tan-sigmoid shape is utilized in the neurons second layer for energizing functions. Also, the piecewise linear shape function is utilized for the output neurons layer. The equation of this sigmoid shape is:

$$f(net_j) = \frac{1}{1 + e^{-c(net_j)}} \quad (4)$$

As displayed in Fig. 3 for faster training, c should be large, and the opposite is correct. The BP algorithm can adjust the weight levels in a multi - layered neural network due to its differentiability.

The training of BP-ANN structure parameters is meant to minimize the output deviation by using the network best weight values. The most widely used strategy is the BP procedure, which is applied in this study, updates the weights in the downward direction (decreasing gradient). In details, the training framework of the proposition structure is illustrated in Fig. 4. An Epoch is the time scale unit used for each trained parameters during the network weights modifications.
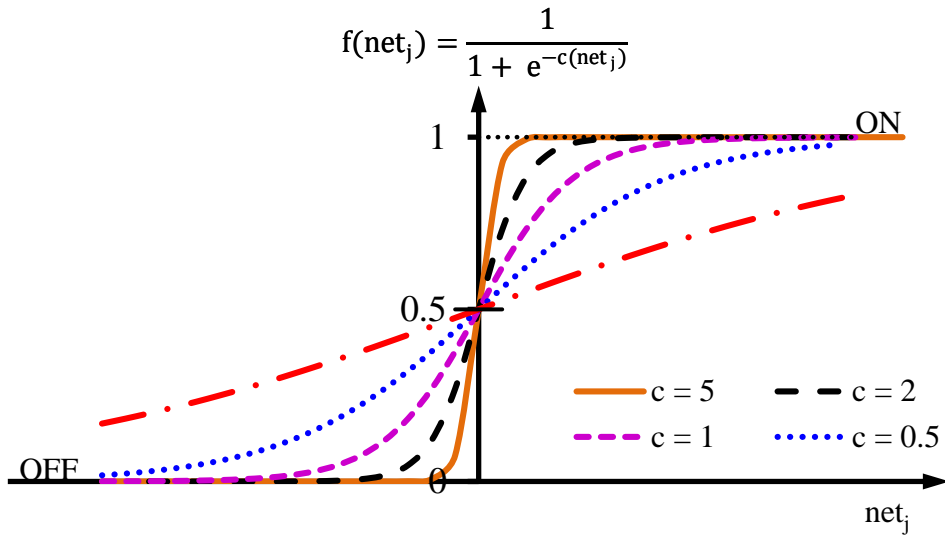
$$f(net_j) = \frac{1}{1 + e^{-c(net_j)}}$$

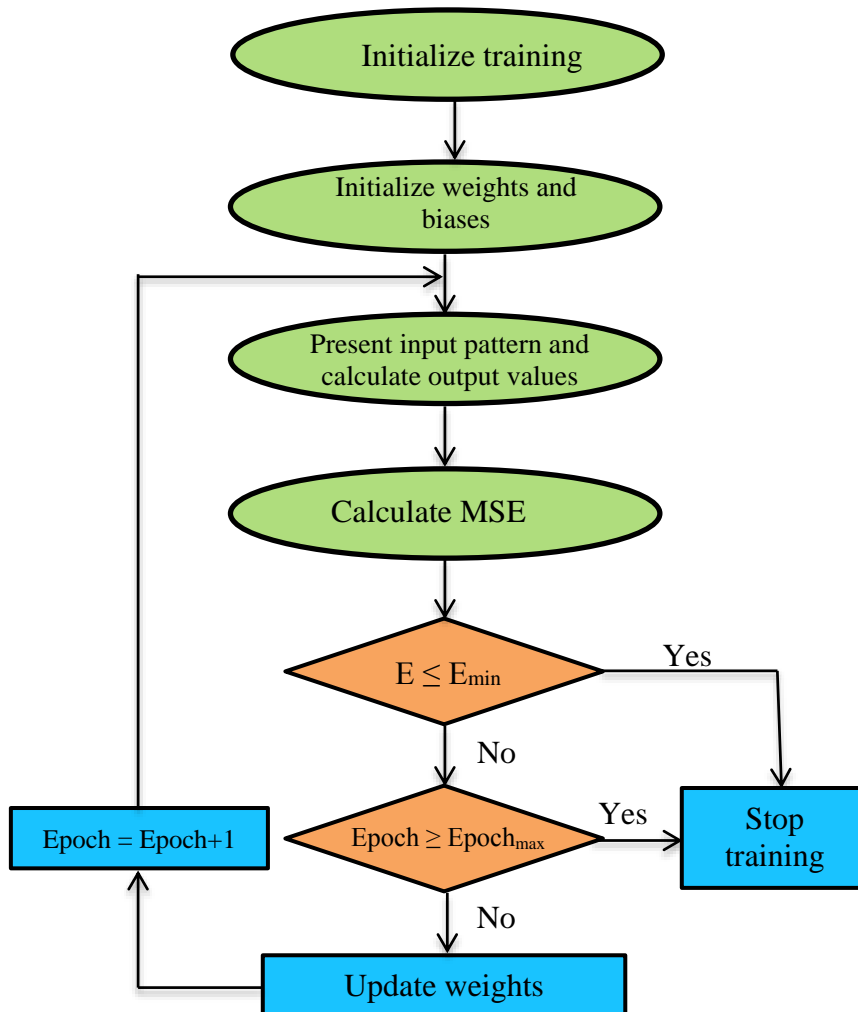**Fig. 3.** The sigmoid activation function changes with different c values.

Fig. 4. A training process flowchart.

It is determined that a 3-layers NNW can converge any complex function with defined required accuracy [28]. In the current training steps, the NW structure has three layers with no need to modify their biases. The training processes are:

1. Forward-propagation phase: $X = [x_1, x_2,..., x_8, x_9]$ propagates from the first layer to the last layer Y.

$$Z_q = f\left(\sum_{j=1}^{n} v_{qj}X_j\right)_{,\ n=9} \tag{5}$$

$$Y = f\left(\sum_{q=1}^{k} w_{iq}Z_q\right) \tag{6}$$

where:

Z_q is the second layer data sets,

f is the agnation function,

V_{qj} is the first-to-second neurons connections weights,

Y is the output of the ANN, and

W_{iq} is the second-to-last neurons connections weights.

2. Back Propagation phase: eq. (7) presents the deviation between the last layer Y, and the goal d:

$$E = \frac{1}{2}\sum_{i=1}^{m}(d_i - y_i)^2 \tag{7}$$

where m is the training points count.

The weights in the second-to-last neurons connections are optimized by utilizing the gradient-descent procedure as follow:

$$\Delta W_{iq} = -\eta\ \frac{\partial E}{\partial W_{iq}} = -\eta\left[\frac{\partial E}{\partial Y}\right]\left[\frac{\partial Y}{\partial net_i}\right]\left[\frac{\partial net_i}{\partial W_{iq}}\right]$$

$$= -\eta\ [d_i - y_i]\ [f'(net_i)][Z_q] = \eta\ \delta_{oi}\ Z_q \tag{8}$$

where η is the training rate.

For modifying the first-to-second correction weights are as follow:

$$\Delta V_{qi} = -\eta\ \frac{\partial E}{\partial V_{qi}} = -\eta\left[\frac{\partial E}{\partial net_q}\right]\left[\frac{\partial net_q}{\partial V_{qj}}\right] = \eta\delta V_{hq}x_i \tag{9}$$

$$\delta_{oi} = -[d_i - y_i][f'(net_i)] \tag{10}$$

$$\delta_{hq} = \left[\frac{\partial E}{\partial Z_q}\right]\left[\frac{\partial Z_q}{\partial net_q}\right] \tag{11}$$

where δ_{oi} is the local and δ_{hq} is the partial deviations.

The process continues to decrease the performance deviation to pre-defined value. The ANN realization is calculated via the linear correlation coefficient (r) and the mean squared error (MSE). As the NWs train its MSE value will be the interactions continue until the power deviation has dropped to a pre-defined value. When the NWs are fully trained, the MSE value approaches zero.

The nine independent inputs, to characterize the ṁ across the capillary tube, are supplied to the second neuron layer. Every neuron connection has modifiable weighting factor connected with it. The solving operations decrease the MSE (goal function) between the trained and the aimed output. The three suggested BP-ANN models are trained and proved with verities of capillary tube geometry, operating conditions, and refrigerant properties as inputs and the refrigerant ṁ as output. The following section presents the results of these models.


4. RESULTS AND DISCUSSION

In the present study, the measurements reported by Jabaraj et al. [26] are utilized in training the three BP-ANN models. Two of the BP-ANN models are constructed for R22 and R407C-R600a-R290 mixture individually, while the third model is general for both refrigerants together. The measurements contain 200 data sets for each refrigerant. 150 data sets from each refrigerant are used to train the two individual models while the reaming 50 data sets are utilized to test the estimation accuracy of the two models. On the other hand, the general model uses 300 data sets (150 data sets for R22 and 150 data sets for R407C-R600a-R290 mixture) to construct and train the model while the rest 100 data sets are utilized to examine the predictive mode of the general model. The mass flow rates estimated by the BP-ANN models are validated against the experimental measurements of Jabaraj et al. [26] as shown in Figs, 5-7. It can be observed from the figures that, the three BP-ANN models are in well agreement with the experimental measurements. Subsequently, the three BP-ANN models are executed to examine their prediction performance as displayed in Figs. 8-10. As can be detected from these figures, the relations between predicted results and measurements are straight lines. This proves the perfect estimation of the models. It is worth emphasizing that the measurements, not utilized in the establishment of the BP-ANN models, are utilized to test the estimation performance of the proposed models.
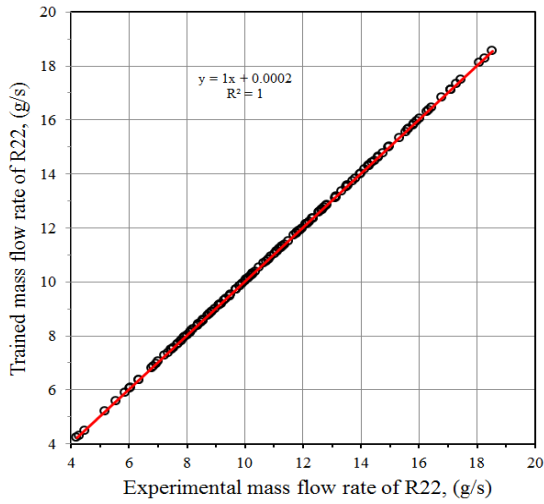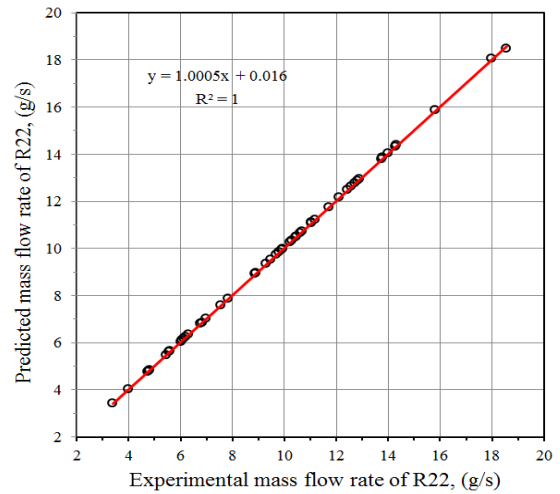
Fig. 5. The BP-ANN model trained data against measured mass flow rates for R22.
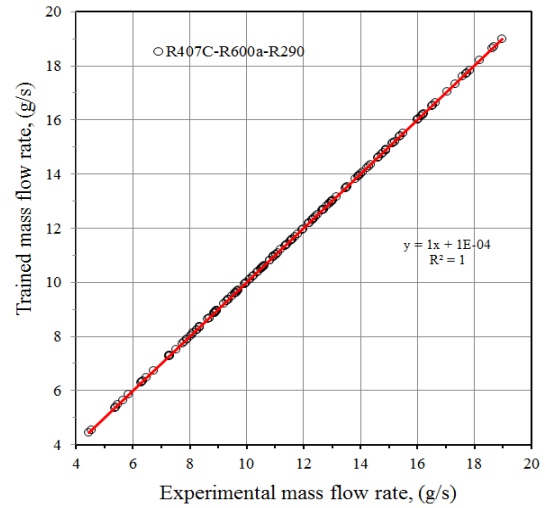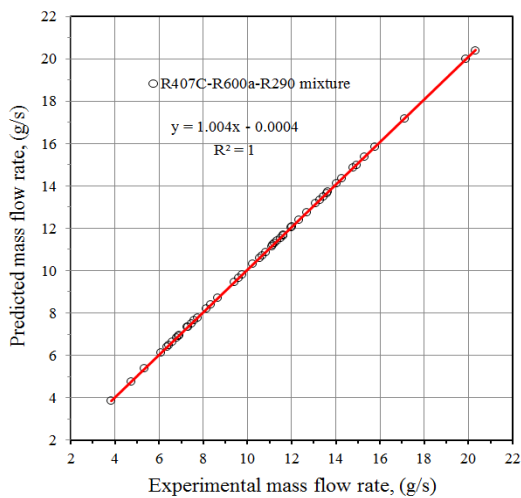

Fig. 6. The BP-ANN model trained data against measured mass flow rates for R407C-R600a-R290 mixture.
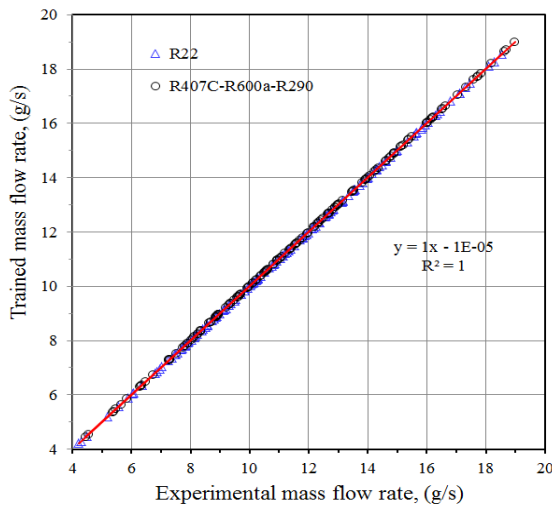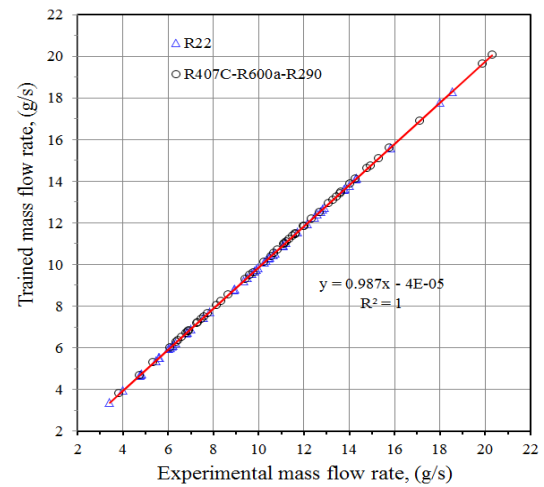

Fig. 7. Trained data of the general BP-ANN model against measured mass flow rates for R22, and R407C-R600a-R290 mixture.

Fig. 8. Predicted data of R22 BP-ANN model against measured mass flow rates.

Fig. 9. Predicted data of R407C-R600a-R290 BP-ANN model against measured mass flow rates.

Fig. 10. Predicted data of the general BP-ANN model against measured mass flow rates for R22 and R407C-R600a-R290.

To assess the precision of the general BP-ANN model for estimation the refrigerant ṁ, the relative differences as functions of capillary tube geometries and working conditions are presented in Fig. 11. As can be noticed from these four figures, the estimated ṁ values are in a very good agreement with the experimental results. The relative differences in the trained model are within $\pm 0.02\%$ for the two inspected refrigerants together. Also, the deviations of the two individual models from the measurements in the trained mode are calculated. The relative differences of the two individual models in the trained mode are within $\pm0.02\%$ and $\pm0.016\%$ for R22, and R407C-R600a-R290 mixture, respectively. The standard and average deviations of the estimation in the trained mode for the general model are 0.006% and 0.003%, respectively. The standard and average deviations of the estimation of the two individual models in the trained mode are 0.006%, 0.0003% for R22, and 0.005%, -0.0003% for R407C-R600a-R290 mixture, respectively. The relative, average, and standard deviations are defined as:

$$\text{Relative difference } E_{Rel}, \text{percent} = \frac{\dot{m}_{Tran} - \dot{m}_{exp}}{\dot{m}_{exp}} \times 100 \quad (12)$$

$$\text{Average deviation } E_{Aver}, \text{percent} = \frac{1}{m}\sum_{1}^{m}\left\{\frac{\dot{m}_{Tran} - \dot{m}_{exp}}{\dot{m}_{exp}} \times 100\right\} \quad (13)$$

$$\text{Standard deviation } E_{S}, \text{percent} = \sqrt{\frac{1}{m}\sum_{1}^{m}(E_{Rel} - E_{Aver})^2} \quad (14)$$

Also, the three models are inspected in the predictive mode outside their establishment ranges. The relative differences of the two individual models and the general model in the predictive mode are within $\pm0.5\%$, $+0.38\%/+0.41\%$, and $-1.28\%/-1.32\%$ for R22, R407C-R600a-R290 mixture, and the two refrigerants together, respectively. The standard and average deviations of the estimation in the predictive mode are 0.11%, 0.23% for R22, 0.006%, 0.4% for R407C-R600a-R290 mixture and 0.007%, -1.3% for two refrigerants together, respectively.
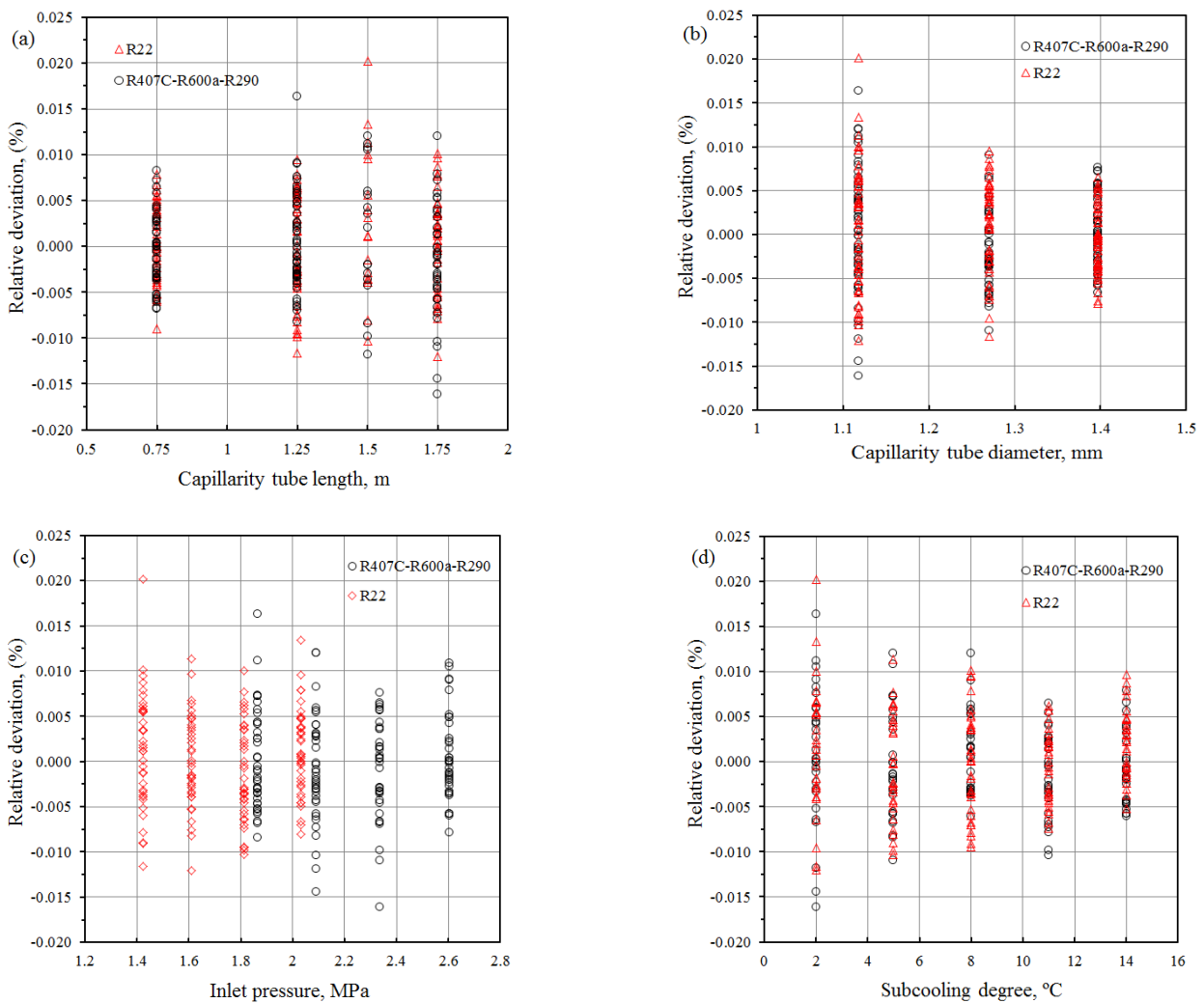
Fig. 11. Relative deviation of the general model results against capillarity tube length (a), capillarity tube diameter (b), inlet pressure (c), and degree of subcooling (d).

Based on these results, the BP-ANN method is a promising tool to estimate ṁ across adiabatic straight capillary tubes. The impacts of capillary tube geometry and operating conditions on the refrigerant ṁ across adiabatic straight capillary tubes will be discussed in the subsequent subsections. Since the general BP-ANN model is more logical than the two individual models; it will be utilized to calculate the refrigerant mass flow in the subsequent sections.

4.1 The impact of capillary tube geometry on mass flow rate

Figure 12 displays the impact of capillary tube geometry on ṁ of R22 and R407C-R600a-R290 mixture. Figure 12a shows the alteration of ṁ as a function of capillary tube diameter for a tube length of 1750 mm, T_{sub} of 8 °C and condenser temperatures of 37, 42, 47, and 52 °C. The increase of capillary tube diameter increases ṁ significantly for both refrigerants. This is attributed to the reduction of pressure drop with increase of capillary tube diameter. For instance, as capillary tube diameter increases from 1.1176 to 1.397 mm

the ṁ growths by about 65% for both refrigerants at 47 °C condenser temperature. As can be noticed from Fig. 12a, the R407C-R600a-R290 mixture mass flow rates are greater than those of R22 and ranged between 1.9 and 5.2% for all examined condenser temperatures and different diameters. Figure 12b displays the alteration of ṁ against the capillary tube length for 42 °C condenser temperature, T_{sub} of 11 °C and capillary tube internal diameter of 1.1176, 1.72, and 1.397 mm. The mass flow rates decrease with the increase of capillary tube length for bot refrigerants. This is because of increase frictional resistance with the tube length. For instance, ṁ decreases with approximately 48% as tube length increases from 750 to 1750 mm with tube diameter of 1.72 mm for both refrigerants. Also, the R407C-R600a-R290 mixture mass flow rates are greater than those of R22 and ranged from 1.75% to 4.5% for all inspected capillary tube lengths and diameters. The lower ṁ of R22 than R407C-R600a-R290 mixture is logically due to the higher viscosity of R22 than R407C-R600a-R290 mixture. Moreover, the higher capillary tube inlet pressure in the case of R407C-R600a-R290 mixture than R22 boosts its ṁ.
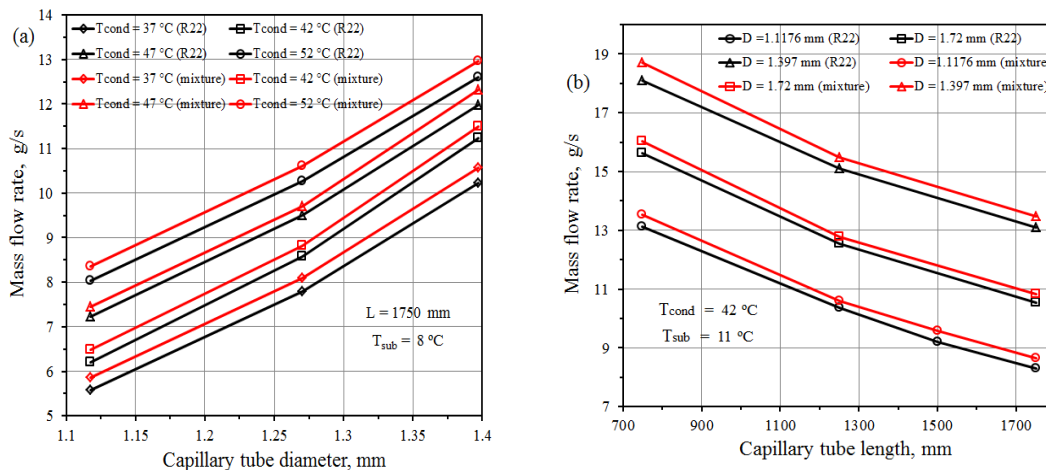

**Fig. 12.** Impact of capillary tube geometry on mass flow rate; tube diameter(a) and tube length (b).

4.2 The impact of operating conditions on mass flow rate

Figure 13 presents the impact of operating conditions on refrigerant ṁ. The alteration of ṁ against the condenser temperature is presented in Fig. 13a for tubes with different diameters, T_{sub} of 5 °C and tube constant length of 1250 mm. The mass flow rates growth with the rise of condenser temperature for both refrigerants under all investigated capillary tube geometries. The tendencies of the mass flow rates are nearly independent of the refrigerants. R22 exhibits lower ṁ than R407C-R600a-R290 mixture under all inspected conditions, due to its lower saturation pressure than R407C-R600a-R290 at the same condenser temperatures. The inlet pressure to the capillary tube in the measurements is set to the saturation pressure conforming to the condenser temperatures of 52, 47, 42, and 37 °C. The refrigerant R407C-R600a-R290 mixture condensing temperature is specified at fixed pressure as the average of bubble and dew points temperatures. The capillary tube exit pressure is adjusted at the saturation

pressure conforming to 7 °C evaporator temperature. The increase of condenser temperature resulting in rise capillary tube inlet pressure, which leads to enhance mass flow rates for both refrigerants. For example, the ṁ increases with nearly 26% as condenser temperature increases from 37 to 52 °C with tube diameter of 1.72 mm for both refrigerants.

The alteration of ṁ against T_{sub} is presented in Fig. 13b for capillary tube diameter of 1.1176 mm, condenser temperature of 42 °C, and various capillary tube lengths. The mass flow rates boost with the increase of T_{sub} for both refrigerants under all investigated capillary tube lengths. The refrigerant at the exit of capillary tube for the flashing of the subcooling inlet will be minor and accordingly there is larger liquid fraction in the capillary tube. The density of refrigerant at the capillary tube entrance increased with the boosting of T_{sub}, which leads to greater refrigerant ṁ at identical volumetric flow. As can be detected from Fig. 13b, the R407C-R600a-R290 mixture mass flow rates are greater than those of R22 and ranged between

1.7% and 4.5% for all inspected T_{sub} and different capillary tube lengths.
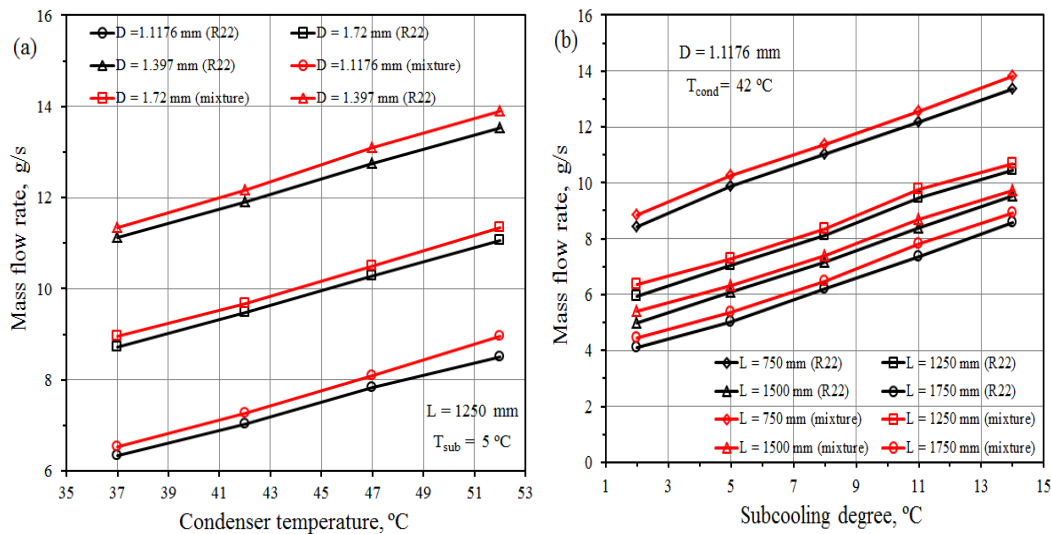
Fig. 13. Impact of operating conditions on mass flow rate; condenser temperature (a) and degree of subcooling (b).

5. CONCLUSIONS

The mass flow rate of R22 and its alternative R407C-R600a-R290 refrigerant mixture across adiabatic straight capillary tube are inspected utilizing back propagation artificial neural network method trained by previously published experimental measurements from open literature. Capillary tube has mainly nine controlling parameters divided into three groups. These groups are capillary tube geometry, refrigerant properties, and working conditions parameters. The geometric parameters are the tube length and diameter. The refrigerant properties parameters are liquid viscosity, liquid specific heat, liquid specific volume, heat of vaporization, and surface tension. The working conditions parameters are the inlet pressure and degree of subcooling. These nine parameters are specified as independent parameters and utilized to establish the BP-ANN models to estimate the mass flow rate across adiabatic straight capillary tubes. Three BP-ANN models are constructed, two separated models for each inspected refrigerant and the third model is a general model for both refrigerants together. The two refrigerants BP-ANN models trained for mass flow rates match perfectly with experimental measurements. These models show relative differences of the trained mass flow rates within ±0.02% and ±0.016% for R22, and R407C-R600a-R290 mixture, respectively. Regarding the general model, the relative differences in the trained mode are within ±0.02% for the two refrigerants. On the same hand, the predictive performance of the three proposed BP-ANN models is inspected as well. It shows well correlation with experimental measurements of the mass flow rates previously published by other authors. The relative differences of the mass flow rates calculated by the three BP-ANN models in the predictive mode from the measurements are within ±0.5%, +0.38%/+0.41%, and -1.28%/-1.32% for R22, R407C-R600a-R290 mixture, and both refrigerants, respectively. The BP-

ANN models are robust tools for estimating the two inspect refrigerants mass flow rates through adiabatic straight capillary tube. The mass flow rate through the capillary tube is affected in various extents by the operating parameters and capillary tube geometry. The impacts of capillary tube geometry and operating conditions on the refrigerant mass flow rate across capillary tube are also investigated and discussed. It is found that, the mass flow rate is directly proportional to the capillary tube diameter, condenser temperature, and degree of subcooling. On the other hand, the mass flow rate is found to be inversely proportional to capillary tube length.

REFERENCES

[1]   B.G. Kim, D.W. Kim, D.C. Lee, Y.C. Kim, Performance of a two-phase injection heat pump with the variation of injection quality and pressure, Int. J. Air-Cond. Refrig. 25 (2) (2017) 1750018.

[2]   N.H. Kim, Application of the natural refrigerant mixture R-290/DME to a soft ice cream refrigerator, Int. J. Air-Cond. Refrig. 24 (4) (2016) 1650027.

[3]   D.A. Elraheim, O.E. Mahmoud, M. Fatouh, Experimental assessment of a domestic split type air-

conditioner working with R410A, Int. J. Air-Cond. Refrig. 24 (4) (2016) 1650021.

[4]   S.K. Dubba, R. Kumar, Flow of refrigerants through capillary tubes: a state-of-the art, Exp. Therm. Fluid Sci. 81 (2017) 370-381.

[5]   F. Ghadiri, M. Rasti, The effect of selecting proper refrigeration cycle components on optimizing energy consumption of the household refrigerators, Appl. Therm. Eng. 67 (2014) 335-340.

[6]   D. Sarker, J.H. Jeong, Development of empirical correlations for non-adiabatic capillary tube based on mechanistic model, Int. J. Refrig., 35 (4) (2012) 974-983.

[7]   B. Saleh, and Ayman A. Aly "Artificial neural network models for depicting mass flow rate of R22, R407C and R410A through electronic expansion valves", Int. J. Refrig., 63 (2016) 113-124.

[8]   C. Melo, R. Ferreira, C.B. Neto, J. Goncalves, M. Mezavila, An experimental analysis of adiabatic capillary tubes, Appl. Therm. Eng., 19 (6) (1999) 669-684.

[9]   C. Melo, R.H. Pereira, Experimental study on adiabatic flow of R-22 alternatives in capillary tubes, in: International Refrigeration and Air Conditioning Conference, Purdue University, 2004, Paper No. 704.

[10] T. Apaydin, H. Heperkan, Experimental investigation of R600a refrigerant flow inside adiabatic capillary tube, Sig. J. Eng. Nat. Sci. 34 (2) (2016) 241-252.

[11] M. Schenk, L.R. Oellrich, Experimental investigation of the refrigerant flow of isobutane (R600a) through adiabatic capillary tubes, Int. J. Refrig., 38 (2014) 275-280.

[12] E. Dirik, C. Inan, M.Y. Tanes, Numerical and experimental studies on adiabatic and nonadiabatic capillary tubes with HFC-134a, in: International Refrigeration and Air Conditioning Conference, Purdue university, 1994, Paper No. 274.

[13] J.J. Meyer, W.E. Dunn, Alternative refrigerants in adiabatic capillary tubes, in: Air Conditioning and Refrigeration Center. College of Engineering, University of Illinois at Urbana-Champaign, ACRC Project 69, 1996.

[14] D.A. Wolf, R.R. Bittle, M.B. Pate, Adiabatic capillary tube performance with alternative refrigerants, ASHRAE final report No. RP-762, 1995.

[15] S.G. Kim, M.S. Kim, S.T. Ro, Experimental investigation of the performance of R22, R407C and R410A in several capillary tubes for air-conditioners, Int. J. Refrig. 25 (5) (2002) 521-531.

[16] J.M. Choi, Y.C. Kim, H.Y. Kim, A generalized correlation for refrigerant mass flow rate through adiabatic capillary tubes, Int. J. Refrig. 26 (8) (2003) 881-888.

[17] J.M. Choi, Y.C. Kim, J.T. Chung, An empirical correlation and rating charts for the performance of adiabatic capillary tubes with alternative refrigerants, Appl. Therm. Eng. 24 (1) (2004) 29-41.

[18] C.L. Zhang, Generalized correlation of refrigerant mass flow rate through adiabatic capillary tubes using artificial neural network, Int. J. Refrig. 28 (4) (2005) 506-514.

[19] M. Rasti, J. H. Jeong, A generalized continuous empirical correlation for predicting refrigerant mass flow rates through adiabatic capillary tubes, Appl. Therm. Eng. 139 (2018) 47-60.

[20] M. Rasti, J. H. Jeong, A generalized continuous empirical correlation for the refrigerant mass flow rate through adiabatic straight and helically coiled capillary tubes, Appl. Therm. Eng. 143 (2018) 450-460.

[21] P. Javidmand, K. A. Hoffmann, Numerical-based non-dimensional analysis of critical flow of R-12, R-22, and R-134a through horizontal capillary tubes, Int. J. Refrig., 58 (2015) 58-68.

[22] L. Yang, W. Wang, A generalized correlation for the characteristics of adiabatic capillary tubes, Int. J. Refrig., 31 (2008) 197-203.

[23] L. Yang, C.L. Zhang, A generalized dimensionless local power-law correlation for refrigerant flow through adiabatic capillary tubes and short tube orifices, Int. J. Refrig., 46 (2014) 69-76.

[24] C.L. Zhanga, L.X. Zhao, Model-based neural network correlation for refrigerant mass flow rates through adiabatic capillary tubes, International Journal of Refrigeration 30 (2007) 690-698.

[25] G. Zhou, Y. Zhang, Y. Yang, X. Wang, Numerical model for matching of coiled adiabatic capillary tubes in a split air conditioner using HCFC22 and HC290, Appl. Therm. Eng. 30 (2010) 1477-1487.

[26] D.B. Jabaraj, A.V. Kathirvel, D.M. Lal, Flow characteristics of HFC407C/HC600a/HC290 refrigerant mixture in adiabatic capillary tubes, Appl. Therm. Eng. 26 (2006) 1621-1628.

[27] E.W. Lemmon, M.L. Huber, M.O. McLinden, Reference Fluid Thermodynamic and Transport Properties-REFPROP Version 9.1., National Institute of Standards and Technology (NIST), Boulder, Colorado, USA 2013.

[28] B. Saleh, Ayman A. Aly, Artificial neural network model for evaluation of the ploughing process performance, International journal of control, automation and systems (IJCAS) 2 (2013) 1-11.

[29] B. Saleh, Ayman A. Aly, Flow control methods in refrigeration systems: A review, International journal of control, automation and systems (IJCAS), 4 (2015) 14-25.

[30] B. Saleh, and Ayman A. Aly "Artificial neural network models for depicting mass flow rate of R22, R407C and R410A through electronic expansion valves", Int. J. Refrig., 63, (2016) 113-124.

[31] K.P. Sudheer, P. Gowda, I. Chaubey, T. Howell, Artificial neural network approach for mapping contrasting tillage practices, Remote Sens. 2 (2010) 579-590.